Article

Electron-Acoustic (Un)Modulated Structures in a Plasma Having (*r*, *q*)-Distributed Electrons: Solitons, Super Rogue Waves, and Breathers

Wedad Albalawi [1], Rabia Jahangir [2], Waqas Masood [3], Sadah A. Alkhateeb [4] and Samir A. El-Tantawy [5,6,*]

1 Department of Mathematical Sciences, College of Science, Princess Nourah bint Abdulrahman University, Riyadh 11656, Saudi Arabia; wsalbalawi@pnu.edu.sa
2 National Centre for Physics (NCP), Quaid-i-Azam University Campus, Shahdra Valley Road 2141, Islamabad 44000, Pakistan; rabia.jahangir@ncp.edu.pk
3 Department of Physics, COMSATS University Islamabad (CUI), Park Road, Chak Shahzad, Islamabad 44000, Pakistan; waqasmasood@comsats.edu.pk
4 Mathematics Department, Faculty of Science, University of Jeddah, Jeddah 23218, Saudi Arabia; salkhateeb@uj.edu.sa
5 Department of Physics, Faculty of Science, Port Said University, Port Said 42521, Egypt
6 Research Center for Physics (RCP), Department of Physics, Faculty of Science and Arts, Al-Mikhwah, Al-Baha University, Al-Baha 1988, Saudi Arabia
* Correspondence: tantawy@sci.psu.edu.eg

Abstract: The propagation of electron-acoustic waves (EAWs) in an unmagnetized plasma, comprising (*r*, *q*)-distributed hot electrons, cold inertial electrons, and stationary positive ions, is investigated. Both the unmodulated and modulated EAWs, such as solitary waves, rogue waves (RWs), and breathers are discussed. The Sagdeev potential approach is employed to determine the existence domain of electron acoustic solitary structures and study the perfectly symmetric planar nonlinear unmodulated structures. Moreover, the nonlinear Schrödinger equation (NLSE) is derived and its modulated solutions, including first order RWs (Peregrine soliton), higher-order RWs (super RWs), and breathers (Akhmediev breathers and Kuznetsov–Ma soliton) are presented. The effects of plasma parameters and, in particular, the effects of spectral indices *r* and *q*, of distribution functions on the characteristics of both unmodulated and modulated EAWs, are examined in detail. In a limited cases, the (*r*, *q*) distribution is compared with Maxwellian and kappa distributions. The present investigation may be beneficial to comprehend and predict the modulated and unmodulated electron acoustic structures in laboratory and space plasmas.

Keywords: non-Maxwellian plasmas; Sagdeev potential; a nonlinear Schrödinger equation; unmodulated solitary waves; rogue waves and breathers

1. Introduction

The electron-acoustic waves (EAWs), first proposed by Fried and Gould in 1961 [1], have been extensively investigated in laboratory experiments [2] and observed in various areas of Earth's magnetosphere, such as geomagnetic tails [3], bow shock [4], Earth's magnetosheath [5], polar cusp [6], and dayside auroral region [7]. The planar symmetric electron acoustic solitary waves (EASWs) in space can either be compressive or rarefactive, and the corresponding amplitude of the electric field ranges from a few mV/m to several 100 mV/m [8]. Moreover, the high frequency region of broadband electrostatic noise (BEN), studied by the satellite missions in various regions of magnetospheres, such as plasma sheet boundary layer (PSBL), the cusp of the magnetosphere, inner magnetosphere, and geomagnetic tail, has been explained successfully in terms of EAWs [9–11].

The EAWs occur in a plasma environment with cold (temperature T_c) electrons that oscillate due to their inertia, hot (temperature T_h) electrons that provide the restoring force,

along with ions that act as a neutralizing background [12]. The frequency of EAWs is usually high and they propagate with a phase velocity greater than thermal velocity of cold electrons and slower than the thermal velocity of hot electrons [13]. However, this mode is strongly Landau-damped and can only contribute when the temperatures of cold and hot electrons are such that $10T_c \lesssim T_h$ and the number density of hot and cold electrons is related as $0 < n_c < 0.8n_e$, where $n_e = n_c + n_h$ [12,14]. Owing to their importance in the magnetosphere, the propagation of nonlinear EAWs has been discussed by several researchers for both unmagnetized [9,15] and magnetized plasma systems [16–19].

Most of the studies in plasma physics mainly relied on the Maxwellian distribution for analyzing the dynamics of constituent particles, until recently. However, it has been observed that the distribution functions deviate significantly from Maxwellian distribution in astrophysical and space plasmas, such as magnetosheath, magnetosphere, ionosphere, solar wind, and interstellar medium [20–22]. Vasyliunas [23] first introduced the kappa or generalized Lorentzian distribution to study the superthermal electrons in the terrestrial magnetosphere. This distribution contains the spectral index κ for measuring the deviation from Maxwellian distribution and reduces to the Maxwellian distribution as $\kappa \to \infty$. Apart from the observations of high energy tails, satellite missions have also reported the electron distributions that exhibit flat top behavior and have different shapes than the Maxwellian distribution in the magnetosheath, terrestrial bow shock, and in the magnetotail [24–27].

The distribution function with both flat top and high energy tails is different from the Maxwellian, kappa, and Cairns distributions. Qureshi et al. [28] first introduced a more general and comprehensive velocity distribution, and named it the double spectral index or generalized (r, q) distribution. Here, the q-index alters the electrons population in the tail of the distribution whereas the r-index determines the electrons at low energies to describe the flat top behavior. Since then, the effects of double spectral index (r, q) on the linear and nonlinear propagation of plasma waves have been studied by a few researchers. Qureshi et al. studied the parallel propagating electromagnetic structures in an (r, q)-distributed plasma and obtained a new dispersion relation for Alfvén waves [28]. Later, Qureshi et al. [29] revisited the study of terrestrial lion roars using the (r, q) distribution, previously studied by Masood et al. [25] for the bi-Maxwellian distribution, and showed sufficient accordance between theory and data. Shah et al. [30] investigated EAWs in the small amplitude limit for planetary magnetospheres and showed that, besides rarefactive solitons, the compressive solitons are also formed for specific values of parameter r, using (r, q) distribution.

The dynamical behaviors of the symmetric arbitrary amplitude unmodulated EASWs have been studied via the Sagdeev potential approach [31], where the dynamics of the solitary pulses are determined through an energy integral equation and the existence domain of the solitons could be estimated from the maximum and minimum Mach numbers. On the contrary, the modulationally unstable region and the propagation of modulated waves can be analyzed by deriving a nonlinear Schrödinger equation (NLSE) [32–38]. These modulated structures include rogue waves (RWs), i.e., Peregrine soliton (first-order RW) [39], and higher-order RWs (super RWs) [40,41], as well as the breathers, i.e., Akhmediev breathers (ABs) [42], and the Kuznetsov–Ma (KM) soliton [43,44], which can be investigated using the derivative expansion method (DEM).

Rogue waves (RWs) are high amplitude pulses with tremendous energy, which appear as a result of the amplitude modulation in the nonlinear dispersive medium [45–56]. RWs are robust and ubiquitous in nature and have been observed in various contexts, such as in biology [57], hydrodynamics [58], optical fibers [59], Bose–Einstein condensates [60], in plasma physics [61], in oceans [62], and in the atmosphere [63]. For a multi-component plasma, Bailung et al. [64] gave the first experimental evidence of first-order RWs, i.e., Peregrine solitons. They showed that the amplitude of the Peregrine soliton becomes thrice the amplitude of nearby waves with a critical concentration of negative ions. Merriche and Tribeche [65] studied electron acoustic RWs in a plasma having Tribeche–Tsallis–Cairns distributed electrons, and observed that nonthermal nonextensive electrons vary in the

region of modulational instability and structure of RWs. Shakir et al. [66] investigated ion acoustic waves and showed that (r, q) distributed electrons modify the domain of modulational instability. Recently, the EAWs have been studied in a collisionless three-component unmagnetized plasma with ions, cold electrons, and (r, q) distributed warm electrons, to show that the indices r and q tend to decrease the growth rate of modulational instability [67].

The breathers are the localized periodic solutions of NLSE [68,69] where the term originates from the fact that most of the breathers oscillate along the spatial or temporal scale. Thus, the ABs are periodic in the space domain, but localized in the time domain, while the KM solitons are localized along the spatial scale, but undergo periodic evolution during propagation. The first experimental observation of KM solitons came out quite late, by Kibler et al. [70] for optical fibers, although, they were proposed theoretically in 1977 [43].

In the present work, the electron-acoustic structures, including the unmodulated (solitary waves) and modulated (rogue waves and breathers) in a non-Maxwellian unmagnetized plasma, comprising (r, q)-distributed hot electrons, cold inertial electrons, and the stationary positive ions, were investigated. The paper is arranged as follows: Section 2 deals with the basic set of governing equations for EAWs in a collisionless unmagnetized plasma. In Section 3, we derive the Sagdeev pseudo-potential and discuss the existence conditions for solitons. The variations of unmodulated solitary structures for plasma parameters is studied in Section 3. Section 4 concentrates on the derivation of NLSE, determining the domain of modulational instability. The rogue waves and the breather solutions of NLSE are analyzed in Section 5. The obtained results are summarized in Section 4.

2. Physical Model and Governing Equations

Consider a collisionless unmagnetized plasma consisting of (r, q) distributed hot electrons (with density n_h), cold inertial electrons (with density n_c), and stationary positive ion (with density n_i). The propagation of wave is considered along x-axis. Accordingly, the condition of charge neutrality reads $n_{i0} = n_{e0} = n_{c0} + n_{h0}$, where n_{h0}, n_{c0} and n_{i0} represent the unperturbed number densities of hot electrons, cold electrons, and positive ions, respectively. The dynamics of EAWs in the plasma model are governed by the set of normalized equations [71], given as

$$\frac{\partial n_c}{\partial t} + \frac{\partial (n_c u_c)}{\partial x} = 0, \tag{1}$$

$$\frac{\partial u_c}{\partial t} + u_c \frac{\partial u_c}{\partial x} - \frac{\partial \phi}{\partial x} + \frac{\sigma}{n_c} \frac{\partial p_c}{\partial x} = 0, \tag{2}$$

$$\frac{\partial p_c}{\partial t} + u_c \frac{\partial p_c}{\partial x} + 3p_c \frac{\partial u}{\partial x} = 0, \tag{3}$$

$$\frac{\partial^2 \phi}{\partial x^2} - \mu n_h - n_c + (\mu + 1) = 0. \tag{4}$$

Here, $\sigma = T_c/T_h$ represents the cold to hot electron temperature ratio. The density n_c, velocity u_c, pressure p_c, and electrostatic potential ϕ are scaled, respectively, by equilibrium number density, $c_s = \sqrt{k_B T_h/m_e}$, $n_{c0} k_B T_c$, and $k_B T_h/e$. Moreover, the space and time variables are, respectively, scaled by the Debye length $\lambda_{De} = (k_B T_h/4\pi n_{c0} e^2)^{1/2}$ and inverse plasma frequency $\omega_{pc}^{-1} = (4\pi n_{c0} e^2/m_e)^{-1/2}$. In the normalized form, the neutrality condition is $n_{i0}/n_{c0} = 1 + \mu$, where $\mu = n_{h0}/n_{c0}$ represents the concentration of hot electrons.

The normalized number density of generalized (r, q)-distributed hot electrons is given by [28]

$$n_h = 1 + \sum_{s=1}^{\infty} \alpha_s \phi^s, \tag{5}$$

where the coefficients α_s are

$$\alpha_1 = \frac{\Gamma\left[q - \frac{1}{2+2r}\right]\Gamma\left[\frac{1}{2+2r}\right](q-1)^{\frac{-1}{1+r}}}{2\beta\Gamma\left[\frac{3}{2+2r}\right]\Gamma\left[q - \frac{3}{2+2r}\right]},$$

$$\alpha_2 = \frac{-\Gamma\left[\frac{-1}{2+2r}\right]\Gamma\left[q + \frac{1}{2+2r}\right](q-1)^{\frac{-2}{1+r}}}{8\beta^2\Gamma\left[\frac{3}{2+2r}\right]\Gamma\left[q - \frac{3}{2+2r}\right]}, \qquad (6)$$

$$\alpha_3 = \frac{\Gamma\left[q + \frac{3}{2+2r}\right]\Gamma\left[\frac{-3}{2+2r}\right](q-1)^{\frac{-3}{1+r}}}{16\beta^3\Gamma\left[\frac{3}{2+2r}\right]\Gamma\left[q - \frac{3}{2+2r}\right]},$$

and so on.

Here $\beta = 3(q-1)^{-1/(1+r)}\Gamma\left[q - \frac{3}{2+2r}\right]\Gamma\left[\frac{3}{2+2r}\right]/(2\Gamma\left[q - \frac{5}{2+2r}\right]\Gamma\left[\frac{5}{2+2r}\right])$ and Γ is the gamma function. The spectral indices "q" and "r" describe the superthermality of high energy particles and the flatness of the curve for low energy particles. Moreover, r and q are sometimes called the flatness and tail parameters. This is the general distribution, in the sense that Maxwellian distribution is retrieved for $r = 0$ and $q \to \infty$ and kappa distribution is recovered for $r = 0$ and $q \to \kappa + 1$. Moreover, for physically meaningful results, the following conditions must be fulfilled: $q > 1$ and $q(r+1) > 5/2$ [28].

3. Sagdeev Potential Approach

The Sagdeev potential approach is devoted to the study of unmodulated arbitrary (but finite) amplitude electron acoustic solitary waves (EASWs). We would like to mention here that the amplitude of KdV type solitons mitigate with its width. However, the EASWs observed by the spacecrafts may show an opposite amplitude–width relationship, i.e., the amplitude of soliton may enhance as its width increases. The solitons given by the Sagdeev pseudo-potential technique exhibit a different property from the KdV solitons, i.e., the amplitude of their solitons may increase or decrease with width depending upon the model and region of application [10,72]. Therefore, the Sagdeev pseudo-potential technique is a better candidate for studying the EASWs belonging to space, although, it may not necessarily show this amplitude–width relation for each plasma model. To apply this approach, we first make use of the following transformation

$$\xi = x - Mt, \qquad (7)$$

for the localized solutions in the moving frame, where $M = v/c_s$ is the normalized Mach number and v is the moving frame velocity. Using transformation (7) and integrating the model Equations (1)–(3) gives

$$u_c = M\left(1 - \frac{1}{n_c}\right),$$
$$u_c = M - \left(M^2 + 2\phi - 3n_c^2\sigma + 3\sigma\right)^{1/2},$$
$$p_c = n_c^3. \qquad (8)$$

Here, the boundary conditions

$$(u_c, n_c, \phi, \phi') \to (0, 1, 0, 0) \text{ at } \xi \to \pm\infty, \qquad (9)$$

have been utilized. Simultaneously solving the above set of Equation (8) yields a biquadratic equation, which can be solved to obtain the following cold electron density

$$n_c = \frac{1}{2}(n_1 \pm n_2), \qquad (10)$$

where $n_{1,2} = \sqrt{\left(2\phi + \left(M \pm \sqrt{3\sigma}\right)^2\right)/3\sigma}$. Substituting the value of n_c into Equation (4) after transformation (7) gives

$$\frac{\partial^2 \phi}{\partial \xi^2} = \mu \sum_{s=1}^{\infty} \alpha_s \phi^s - 1 + \frac{1}{2}(n_1 - n_2) = -\frac{dV(\phi)}{d\phi}. \tag{11}$$

Multiplying Equation (11) by $d\phi/d\xi$ and integrating once over ξ, we finally get the pseudo-energy balance equation

$$\frac{1}{2}\left(\frac{d\phi}{d\xi}\right)^2 + V(\phi) = 0, \tag{12}$$

Equation (12) describes the energy integral for an oscillating particle with unit mass and velocity $d\phi/d\xi$ in a potential well $V(\phi)$ at the position ϕ. The normalized Sagdeev pseudo-potential $V(\phi)$ is then evaluated to be

$$V(\phi) = -\mu \sum_{s=1}^{\infty} \frac{\alpha_s \phi^{s+1}}{s+1} + \phi + \frac{1}{6\sqrt{3\sigma}}\left[\left(M + \sqrt{3\sigma}\right)^3 - \left(M - \sqrt{3\sigma}\right)^3\right]$$
$$+ \frac{1}{6\sqrt{3\sigma}}\left[-\left(2\phi + \left(M + \sqrt{3\sigma}\right)^2\right)^{3/2} + \left(2\phi + \left(M - \sqrt{3\sigma}\right)^2\right)^{3/2}\right] \tag{13}$$

Therefore, the Sagdeev pseudo-potential shows variation with the Mach number, the density ratio μ, the temperature ratio σ,, and the nonthermality parameters (r, q) through the coefficients α_s, i.e., $V(\phi) = V(\phi, M, \sigma, \mu, r, q)$.

For the existence of EASWs, the following conditions must be satisfied

(i) $V(\phi)|_{\phi=0} = V(\phi)|_{\phi=\phi_{max}} = dV(\phi)/d\phi|_{\phi=0} = 0$,
(ii) $d^2V(\phi)/d\phi^2|_{\phi=0} < 0$ gives the minimum/critical Mach number,

where ϕ_{max} is the maximum value at which the curve of potential $V(\phi)$ crosses the ϕ-axis for $\phi \neq 0$. The particles oscillate between the origin and the maximum position (ϕ_{max}). The condition for minima (which describes $V(\phi)$ to be a potential well, rather than a hill) gives

$$\left.\frac{d^2V(\phi, M, \sigma, \mu, r, q)}{d\phi^2}\right|_{\phi=0} = -\mu\alpha_1 + \frac{1}{M^2 - 3\sigma} < 0, \tag{14}$$

which gives $M(\mu, \sigma, r, q) > M_{min} = \sqrt{\frac{1}{\mu\alpha_1} + 3\sigma}$. Note the range of the Mach number changes by changing the hot to cold electron concentration, cold to hot electron temperature ratio, and the electron distribution. Furthermore, note that the value of α_1 would be different for different electron velocity distributions. The maximum value of M is attained from the fact that cold electron density becomes complex at $\phi = \phi_{max}$ that gives $\phi_{max} = -\left(M - \sqrt{3\sigma}\right)^2/2$ for which the Sagdeev potential given by Equation (13) becomes

$$V(\phi)|_{\phi=\phi_{max}} = -\mu \sum_{s=1}^{\infty} \frac{\alpha_s}{s+1}\left[-\frac{1}{2}\left(M - \sqrt{3\sigma}\right)^2\right]^{s+1}$$
$$- \frac{1}{2}\left(M - \sqrt{3\sigma}\right)^2 + M^2 + \sigma - \frac{4}{3}M^{3/2}(3\sigma)^{1/4}. \tag{15}$$

Solving $V(\phi)|_{\phi=\phi_{max}} = 0$ gives us the maximum value of the Mach number M_{max}. Figure 1 shows the curves for maximum (upper) and minimum (lower) Mach numbers, so that the admissible values of the Mach numbers are confined within the region between those curves. These permitted values $[M_{min}, M_{max}]$ define the existence domain of EASWs.

Further, we check the variation of the permitted domain with the variation of number densities of hot electrons μ, temperature ratio σ, and the nonthermal parameters (r, q). Comparison of Figure 1a,b illustrate that increasing the concentration of hot electrons, μ, not only reduces the allowed region, but also shifts it to lower values of the Mach numbers. The increasing electron temperature ratio, σ, on the other hand shrinks the region $[M_{\min}, M_{\max}]$, but shifts to the higher values of Mach numbers as can be seen from Figure 1a,c. Moreover, enhancing the flatness parameter r broadens and shifts upward the permitted region of Mach numbers, as illustrated by the comparison of Figure 1a,d. Figure 1e,f describe the comparison of the (r, q) distribution with those of kappa and Maxwellian distributions. Thus, the comparison of Figure 1a,e shows that the existence region of solitary structures not only shrinks, but also shifts to lower values of Mach numbers for kappa distribution. However, as the value of kappa increases, it shifts to higher values of Mach numbers. Furthermore, Figure 1f illustrates that the permitted domain of the existence of solitons for Maxwellian limits not only shifts, rapidly, to lower values of Mach numbers with an increasing ratio μ, but also gets shrunk. The upshot of this analysis is that changing the hot electron distribution function alters the existence domains of the formation or propagation of the electron acoustic solitary structures.
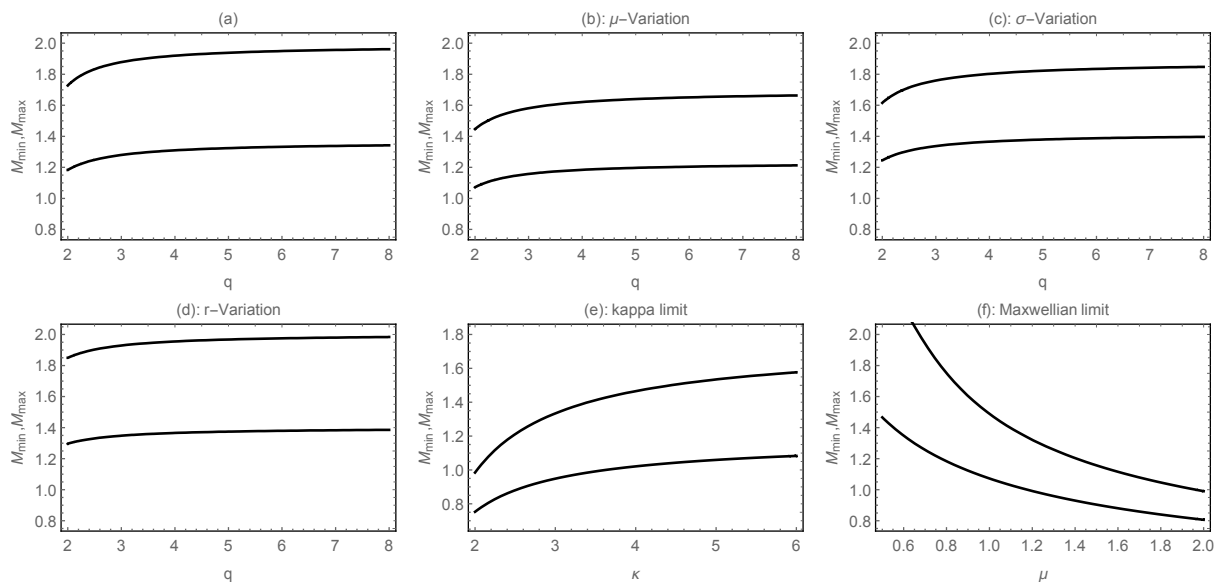

Figure 1. Variation of $M_{\min}$ and $M_{\max}$ versus q to determine the existence domain of EASWs ($M_{\min} < M < M_{\max}$). (**a**) for $(\mu, r, \sigma) = (0.8, 1, 0.05)$, (**b**) for $(\mu, r, \sigma) = (1, 1, 0.05)$, (**c**) for $(\mu, r, \sigma) = (0.8, 1, 0.1)$, (**d**) for $(\mu, r, \sigma) = (0.8, 1.5, 0.05)$, (**e**) for $(\mu, \sigma) = (0.8, 0.05)$ of kappa distribution (**r = 0** and $q \to \kappa + 1$) and (**f**) for $\sigma = 0.05$ of Maxwellian distribution (**r = 0** and $q \to \infty$).

4. Unmodulated Electron-Acoustic Solitary Waves

Before proceeding to the parametric analysis of EASWs, it is important to mention that the present plasma model supports only rarefactive EASWs, although the compressive solitary structures have also been observed in space by the spacecrafts for EAWs. However, we have only used a simple model to study EASWs and compressive structures have been predicted theoretically under certain conditions [15,73]. The values of relevant physical parameters (μ, σ, q) are chosen to minimize the Landau damping of EASWs and are found to correspond to the ones observed in various regions of space, specifically for the plasmas present in terrestrial magnetosphere. Moreover, the flat topped distribution $(r > 0)$ is chosen rather than spiky distribution $(r < 0)$, since most of space data support the flat topped distribution.

Figure 2a demonstrates the relation between the Sagdeev pseudo-potential $V(\phi)$ and the hot electron concentration μ. It is shown that increasing μ leads to the enhancement of the depth and width of the Sagdeev potential. The behavior of the corresponding

solitary waves can be predicted from that of the Sagdeev pseudo-potential profiles. The enhancement of the depth of potential profile corresponds to the reduction of width of that soliton structure, whereas, the amplitude of soliton structure increases if the width of the Sagdeev potential increases. The numerically plotted EASWs corresponding to this Sagdeev potential in Figure 2b show that the increasing concentration of hot electrons enhances the amplitude of solitons but mitigates their width.
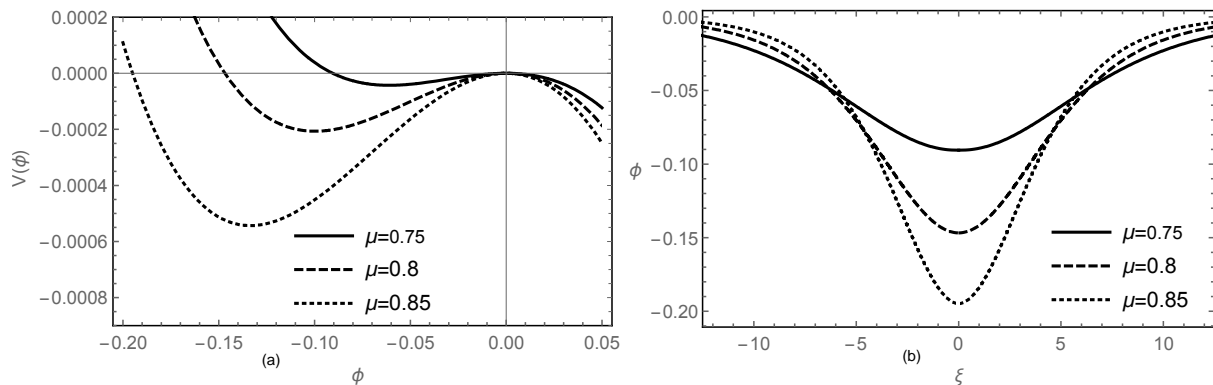

Figure 2. Effect of μ on (**a**) the Sagdeev pseudo-potential $V(\phi)$ and (**b**) the electrostatic potential ϕ of EASWs with $(q, r, \sigma, M) = (2, 1, 0.05, 1.27)$.

Figure 3a,b exhibit the variation of Sagdeev pseudo-potential with the ratio of temperature of cold to hot electrons σ. One can see that increasing the ratio σ reduces the depth and width of the potential well. Furthermore, the amplitude of the corresponding EASWs also reduces with the enhancement of the temperature of cold electrons. Physically, increasing (decreasing) of the amplitude of the EASWs with increasing value of μ (σ) is related to the fact that this mode becomes highly Landau damped with the increase of concentration and temperature of the cold electrons. Figure 4a,b elucidate the effects of spectral index r on the Sagdeev pseudo-potential and on the corresponding solitons. It shows that increase in the values of the flatness parameter r ($r > 0$) reduces the depth and width of the Sagdeev potential. Moreover, the amplitude of the EASWs enervates whereas the width enhances by increasing the number of low energy electrons. It should be pointed out here that compressive EASWs have been predicted for a few negative values of parameter r [30]; however, the negative values of r correspond to a spiky (r, q) distribution, which is yet to be observed and, therefore, not included in this study.
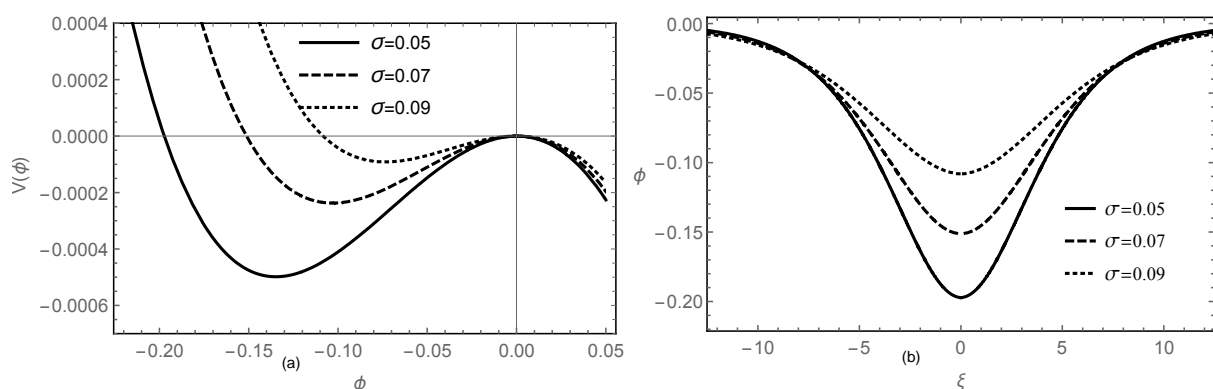

Figure 3. Effect of σ on (**a**) the Sagdeev pseudo-potential $V(\phi)$ and (**b**) the electrostatic potential ϕ of EASWs with $(\mu, q, r, M) = (0.8, 2, 1, 1.3)$.
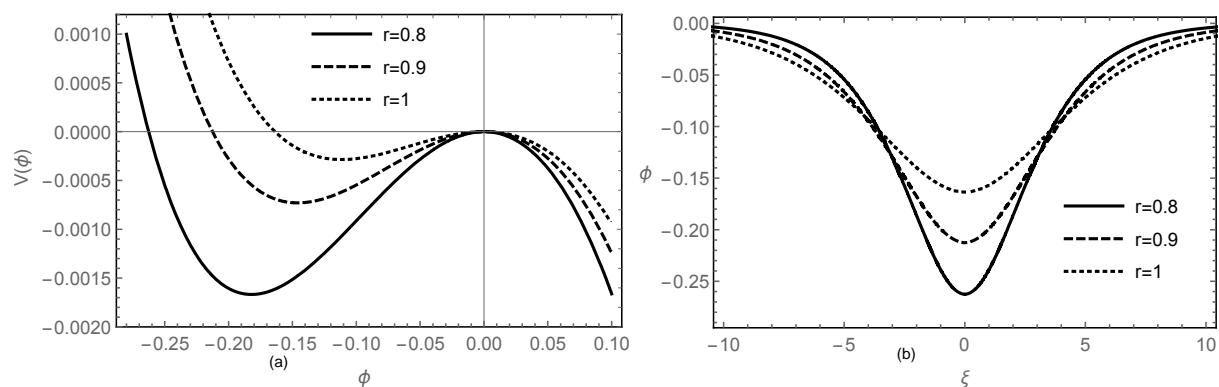
Figure 4. Effect of r on (**a**) the Sagdeev pseudo-potential $V(\phi)$ and (**b**) the electrostatic potential ϕ of EASWs with $(\mu, q, \sigma, M) = (0.8, 2, 0.05, 1.28)$.

Figure 5a depicts the variation of normalized Sagdeev pseudo-potential with increasing spectral index q, which is tantamount to decreasing the energetic electrons in the tail or the electrons in the region of low phase space density. The plot demonstrates that increasing the index q reduces the depth of the Sagdeev potential and shrinks the width of the potential well. The corresponding EASWs in Figure 5b show that increasing the q-value mitigates the amplitude of solitons. Figure 5a further manifests the Maxwellian behavior of the potential well when $r = 0$ and $q \longrightarrow \infty$ and the kappa behavior when $r = 0$ and $q \longrightarrow \kappa + 1$ (where $2 < \kappa < 6$ for space plasmas) and compares it with (r, q) distribution. The Sagdeev potential is deepest and widest for kappa distribution, intermediate for (r, q) distribution (with low r and q values), and Maxwellian distribution, whereas it is most shallow and narrow for (r, q) distribution having a flat top and Maxwellian tail. Figure 5b of corresponding EASWs show that amplitude is largest for kappa distribution and smallest for (r, q) distribution with less energetic electrons in the tail and increasing low energy electrons. In a nutshell, we learn from Figure 5a,b that pumping in, or increasing the number of electrons in low regions of phase space density, enervate the amplitude of the EASWs and increasing the superthermal electrons in high regions of phase space density, invigorates the amplitude of EASWs. Note that the amplitude of the EASWs for kappa distribution is higher than the generalized (r, q) distribution, because, over there, we only enhance the tail population, leaving the percentage of low energy electrons unchanged as opposed to (r, q) distribution, where the percentage of both the high and low energy electrons is changed and, hence, the observation of increased mitigation in the amplitude in this case.
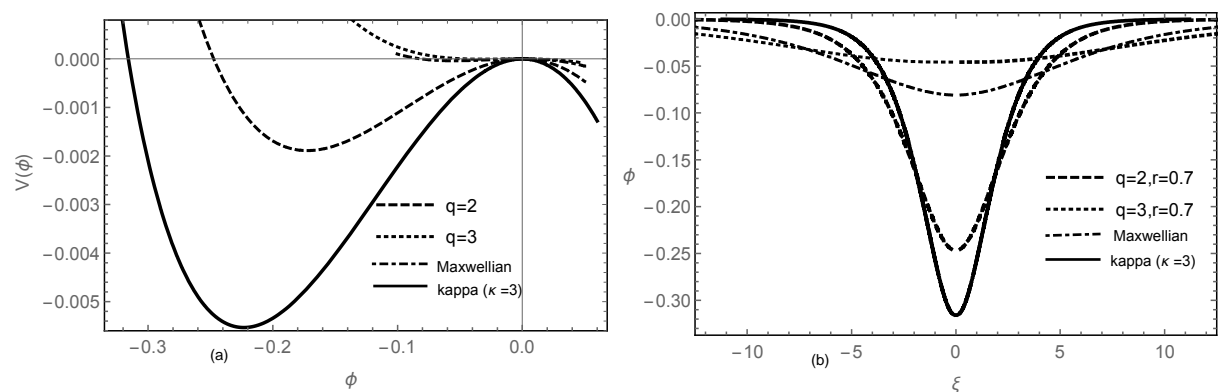

Figure 5. Effect of q on (**a**) the Sagdeev pseudo-potential $V(\phi)$ and (**b**) the electrostatic potential ϕ of EASWs with $(\mu, \sigma, r, M) = (0.8, 0.06, 0.7, 1.25)$ for dotted and dashed curves, $(\mu, \sigma, M) = (0.8, 0.06, 0, 1.25)$ for dotted-dashed curve (Maxwellian distribution $r = 0$, $q \to \infty$) and $(\mu, \sigma, M, \kappa) = (0.8, 0.06, 1.25, 3)$ for solid curve (kappa distribution $r = 0$, $q \to \kappa + 1$).

5. Nonlinear Schrödinger Equation and Modulational Instability

In order to study nonlinear modulated structures, such as Peregrine solitons (first-order RWs) and higher-order RWs (super RW) in the present plasma model, NLSE has to be derived. The derivative expansion method (DEM) is employed to obtain the NLSE. Accordingly, the following stretchings for the independent variables (x, t) and expansions for the dependent quantities are, respectively, introduced [32–35,74,75]:

$$X = \varepsilon(x - \lambda t), \ T = \varepsilon^2 t, \tag{16}$$

and

$$\mathbb{R}(x,t) = \mathbb{R}^{(0)} + \sum_{m=1}^{\infty} \varepsilon^m \sum_{l=-m}^{m} \mathbb{R}_{cl}^{(m)}(X,T)e^{il\Theta}, \tag{17}$$

with $\mathbb{R}(x,t) \equiv [n_c, u_c, \phi]$, $\mathbb{R}_{cl}^{(m)}(X,T) \equiv \left[n_{cl}^{(m)}, u_{cl}^{(m)}, \phi_l^m \right]$, $\mathbb{R}^{(0)} \equiv [1,0,0]$, and $\Theta = (kx - \omega t)$, where k and ω represent the normalized wave number and frequency of the carrier waves, respectively. The dependent quantities $\mathbb{R}_{cl}^{(m)}(X,T)$ must satisfy the reality condition, i.e., $\mathbb{R}_{-l}^{(m)} = \mathbb{R}_l^{*(m)}$, where the asterisk indicates the conjugate of complex quantities. According to the stretching (16) and the derivative expansion method (DEM), the following operators are introduced

$$\begin{cases} \frac{\partial}{\partial t} \to \frac{\partial}{\partial t} - \varepsilon\lambda\frac{\partial}{\partial X} + \varepsilon^2\frac{\partial}{\partial T}, \\ \frac{\partial}{\partial x} \to \frac{\partial}{\partial x} + \varepsilon\frac{\partial}{\partial X}. \end{cases} \tag{18}$$

Using the expansions given by Equation (17) and the differential operators given by (18) into the governing Equations (1)–(5), and after several tedious, long, but simple calculations, a system of reduced equations with different orders of ε will be obtained. We only mention the basic steps to solve this system in order to obtain the NLSE:

The coefficient of $e^{i\Theta}$ for the first-mode ($m = 1$) gives the linear dispersion relation

$$\omega = \sqrt{3\sigma k^2 + \frac{k^2}{\alpha_1 + k^2}}.$$

The coefficient of $e^{i\Theta}$ for the second-mode ($m = 2$) denotes the velocity of the wave packets (group velocity)

$$\lambda = 6\sigma k\omega + \frac{\omega^2 - \omega^4 - 9\sigma^2 k^4}{k\omega} \equiv \frac{\partial\omega}{\partial k}. \tag{19}$$

The coefficient of $e^{i\Theta}$ for the third-mode ($m = 3$) gives the compatibility condition and the solution of this condition leads to the following NLSE [32–35]

$$i\frac{\partial\Phi}{\partial T} + P\frac{\partial^2\Phi}{\partial X^2} + Q|\Phi|^2\Phi = 0. \tag{20}$$

Here, $\Phi \equiv \phi_1^{(1)}$ and the coefficients of the nonlinearity and dispersion terms are, respectively, given by

$$\begin{cases} P = \frac{A_2}{A_1} \equiv \frac{1}{2}\frac{\partial^2\omega}{\partial k^2}, \\ Q = \frac{A_3}{A_1}, \end{cases} \tag{21}$$

with

$$A_1 = -\frac{2k^2\omega}{Z^2},$$

$$A_2 = 1 + \frac{(\lambda k - \omega)}{Z^3}\left(3\lambda\sigma k^3 - 9\omega\sigma k^2 + 3\lambda\omega^2 k - \omega^3\right),$$

$$A_3 = -2\alpha_2 S_4 - 2\alpha_2 C_4 - 3\alpha_3 + \frac{k^6\omega^2}{Z^4} + \frac{12\sigma C_2 k^5}{\omega Z^2} + \frac{k^2(C_1 - S_1)}{Z}$$

$$- \frac{k^2}{Z^2}\left[C_1\left(3\sigma k^2 - 2\omega^2\right) + k^2(\sigma C_3 + 2C_4) - 2\omega k S_2 + 3\sigma k^2(S_1 - S_3)\right], \quad (22)$$

where

$$C_1 = \frac{k^2}{2Z^3}\left(-3k^2\left(k^2\sigma + \omega^2\right) + 2Z^2 C_4\right),$$

$$C_2 = \frac{k\omega}{2Z^3}\left(-k^2\left(9k^2\sigma + \omega^2\right) + 2Z^2 C_4\right),$$

$$C_3 = \frac{3k^2}{2Z^3}\left(k^2\left(3k^2\sigma - 5\omega^2\right) + 2Z^2 C_4\right),$$

$$C_4 = \frac{1}{2Z^2}\left(\frac{2\alpha_2 Z^3 - 3k^2\left(k^2\sigma + \omega^2\right)}{\alpha_1 Z + k^2(4Z + 1)}\right),$$

and

$$S_1 = \frac{1}{Z^2\lambda(\lambda^2 - 3\sigma)}\left[k^2\left\{-Z\lambda_{ph} + \omega\left(k\lambda^2 + 6k\sigma + \lambda\omega\right)\right\} - Z^2\lambda S_4\right],$$

$$S_2 = \frac{1}{Z^2(\lambda^2 - 3\sigma)}\left[k^2\left\{-Z\lambda + \omega\left(-k\lambda^2 + 12k\sigma + \lambda\omega\right)\right\} - Z^2\lambda S_4\right],$$

$$S_3 = \frac{3}{Z^2(\lambda^2 - 3\sigma)}\left[k^2\{-Z + \omega(3k\lambda + \omega)\} - Z^2 S_4\right],$$

$$S_4 = \frac{1}{Z^2\lambda^2(-1 + \alpha_1(\lambda - 3\sigma))}\left(\begin{array}{c}k^3\omega\left(\lambda^2 + 6k\sigma\right) + k^2\lambda\left(-Z + \omega^2\right) \\ -2Z^2\alpha_2\lambda\left(\lambda^2 - 3\sigma\right)\end{array}\right),$$

$$Z = \left(3k^2\sigma - \omega^2\right).$$

Equation (20) is completely integrable and supports many nonlinear modulated structures. The sign of the product PQ gives the necessary and sufficient criteria for determining the stable and unstable regions of the envelope structures. Therefore, for $PQ < 0$, the modulated stable structures, such as dark solitons, exist. However, for $PQ > 0$, the nonlinear structures turn out to be unstable and the bright soliton, Peregrine soliton (first-order RWs), super RWs (higher-order RWs), breather structure (Kuznetsov–Ma (KM) soliton, Akhmediev breathers (ABs)), cnoidal waves (CWs), etc., can be generated. To restrict the regions of (in)stability for the modulated EAWs and their dependence on various physical parameters, we will draw the relationship between the critical wave number k_c (which is the wave number that separates both stable and unstable regions, and the product $PQ = 0$ at k_c) and the relevant physical parameters in Figure 6. It is shown from Figure 6a,b that increasing the concentration of the hot electrons μ would reduce the instability region and shift it to the higher values of k. On the contrary, the instability region expands and shifts to smaller values of the wave number with the increasing values of the temperature ratio, σ, of the electrons, as illustrated in Figure 6c,d. Furthermore, the plots illustrate that the wave number shifts to slightly lower values by increasing the values of both the flatness parameter r and the tail parameter q. The limiting cases of kappa and Maxwellian distributions have been plotted in Figure 6e,f. Thus, for the kappa distribution function ($r = 0$ and $q \to \kappa + 1$), the unstable region shifts to higher values of k and expands tremendously with increasing kappa values. Moreover, for the Maxwellian limit ($r = 0$ and

$q \longrightarrow \infty$), the unstable region expands for lower values of the ratio of the concentration of electrons μ and shifts to lower values of the wave number as compared to the kappa distribution.
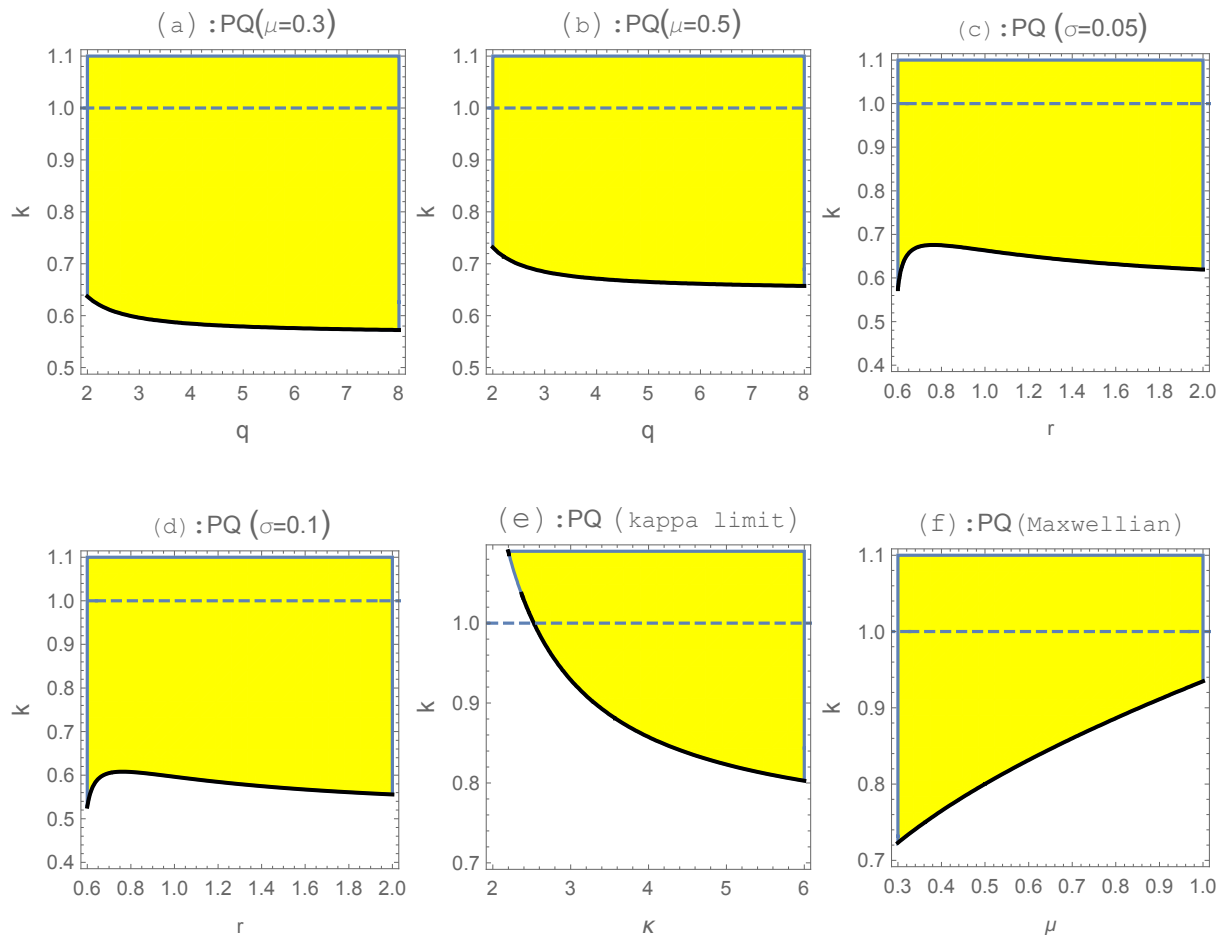

Figure 6. Regions of stable (white color) and unstable (yellow color) modulated EAWs for different values of the physical parameters. The product PQ is plotted: (**a**) in the plane (k, q) for $(\mu, \sigma, r) = (0.3, 0.1, 1)$, (**b**) in the plane (k, q) for $(\mu, \sigma, r) = (0.5, 0.1, 1)$, (**c**) in the plane (k, r) for $(\mu, \sigma, q) = (0.3, 0.05, 3)$, (**d**) in the plane (k, r) for $(\mu, \sigma, q) = (0.3, 0.1, 3)$, (**e**) for $(\mu, \sigma) = (0.3, 0.1)$ of kappa distribution and (**f**) for $\sigma = 0.1$ of Maxwellian distribution.

6. Electron Acoustic RWs and Breathers

In this section, the modulated structures that can exist and propagate in the unstable regions ($PQ > 0$), such as RWs and breathers [45], can be investigated. The physical reason behind development of these structures is the nonlinear growth of resultant instability that causes the accumulation of a large amount energy into a small temporal–spatial region. The compact analytical formula for first-order RW solution and breathers solution to Equation (20) reads [42]:

$$\Phi = \sqrt{\frac{2P}{Q}} \left[1 + \frac{2(1 - 2\rho) \cosh(f_1 \tilde{T}) + i f_1 \sinh(f_1 \tilde{T})}{\sqrt{2\rho} \cos(f_2 X) - \cosh(f_1 \tilde{T})} \right] \exp(i\tilde{T}), \tag{23}$$

where, $\Phi \equiv \Phi(X, \tilde{T})$, $\tilde{T} = 2PT$, and ρ is the control switch responsible for determining the type of wave solution according to the two quantities $f_1 = \sqrt{2\rho f_2^2}$ and $f_2 = \sqrt{4(1 - 2\rho)}$. If $0 < \rho < 1/2$, the solution (23) becomes the ABs solution Φ_{ABs} with period $2\pi/f_2$ as shown in Figure 7a, while the KM soliton solution Φ_{KM} will be generated if $\rho > 1/2$ as shown in Figure 7b, and finally, the solution (23) can become the first-order RW solution

at $\lim \Phi(\rho \to 1/2) = \Phi_{RW_1}$ as illustrated in Figure 7c. Figure 7 shows that the ABs are localized in the time domain, but periodic in the space domain, while the KM solitons have an opposite behavior, i.e., they are localized in the space domain, but periodic in the time domain. Peregrine solitons are the limiting case of both ABs and KM solitons, as they are localized structures along both spatial and temporal scales. Furthermore, the super RW solutions are given by

$$\Phi_j = \sqrt{\frac{2P}{Q}} \left[(-1)^j + \frac{G_j + i\tilde{T}H_j}{D_j} \right] e^{(i\tilde{T})}, \tag{24}$$

where j expresses the jth-order of the RW solutions. The function G_j, H_j, and $D_j \neq 0$ represent the polynomials in terms of slow independent variables X and $\tilde{T}$ and their values could be found in many Reference [41]. It is important to mention here that the super RWs are also localized in both spatial and temporal domains. The super RWs (here we take the second- and third-order as examples) have the same qualitative behavior as the first-order RWs, but they differ in the quantitative behavior, so that the super RWs are more spiky (narrow width and large amplitude) than the first-order RWs, as is evident in Figure 8. In this figure, the comparison between the first three-orders of solution (24) is considered. The amplification of first-order RWs reads $\Phi_{1\max}(X = 0, \tilde{T} = 0) = 3\sqrt{2P/Q}$. In general, the amplifications of all orders RWs could be written in the following form: $\Phi_{j\max}(X = 0, \tilde{T} = 0) = \sqrt{2P/Q}(2j + 1)$. The dependence of first-order RWs on the concentration of hot electrons μ, the electron temperature ratio σ, the wave number k, and the nonthermal parameters (r, q) is explained in Figure 9. It is clear that with increasing μ, both the amplitude and the width of RWs increase as shown in Figure 9a. On the contrary, the impact of the temperature ratio σ on the RWs profile show the opposite behavior, i.e., both amplitude and width decay with increasing σ as elucidated in Figure 9b. Moreover, an increase in nonthermal parameters (r, q) and the the wavenumber k lead to reduction of both the amplitude and width of the RWs as shown in Figure 9c–f. The Maxwellian and kappa distributions have also been investigated in Figure 9d,e, which show that the amplitude of RWs is higher for Maxwellian distribution in comparison with kappa distributed electrons. However, it should be noted that when we draw a comparison between different electron distribution functions for the electron acoustic RWs, the graphs for kappa distribution are plotted for different values of μ as the unstable regime of RWs is different for different electron velocity distribution functions. The reason being that no common region with the same values of plasma parameters is defined for Maxwellian and kappa distributions as can be seen from Figure 6e,f. Furthermore, Figure 9d shows that amplitude is higher for generalized (r, q) distributed electrons with less flat top (lower values of r) and non-Maxwellian tail (low q value) by comparison with the Maxwellian case ($q \to \infty, r = 0$). Physically, enhancement of the amplitude of RWs with a physical parameter determines the increase of the transfer of energy from the surrounding medium to the system, while mitigation of the amplitude means a decrease of the energy transfer from the surrounding waves to the system and increase of the energy dissipation to the surrounding medium.
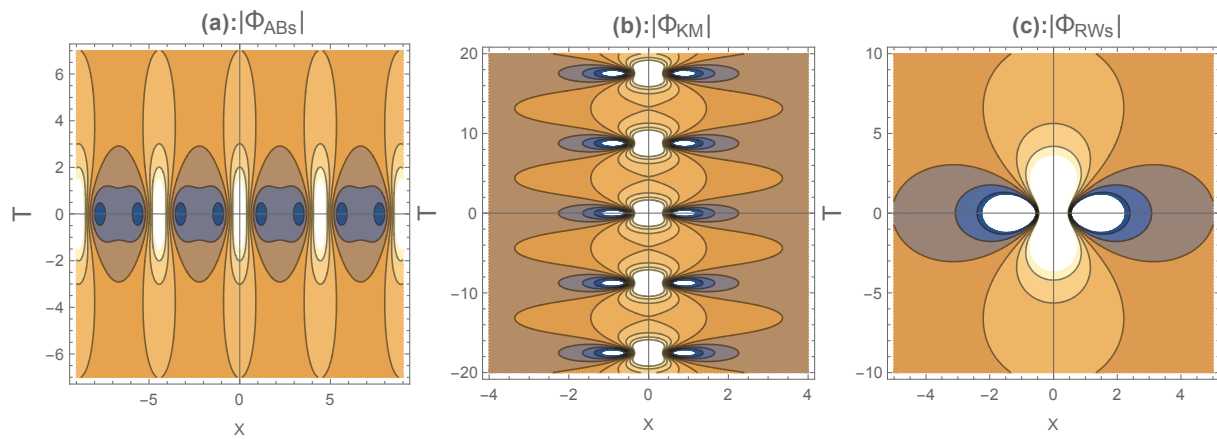
Figure 7. The profile of (**a**) Akhmediev breathers (ABs) $|\Phi_{ABs}|$, (**b**) Kuznetsov–Ma (KM) soliton (KM) $|\Phi_{KM}|$, (**c**) Rogue waves (RWs) $|\Phi_{RWs}|$ is plotted in the plane (X, T) for $(\mu, \sigma, q, r, k) = (0.3, 0.1, 4, 1, 0.8)$.
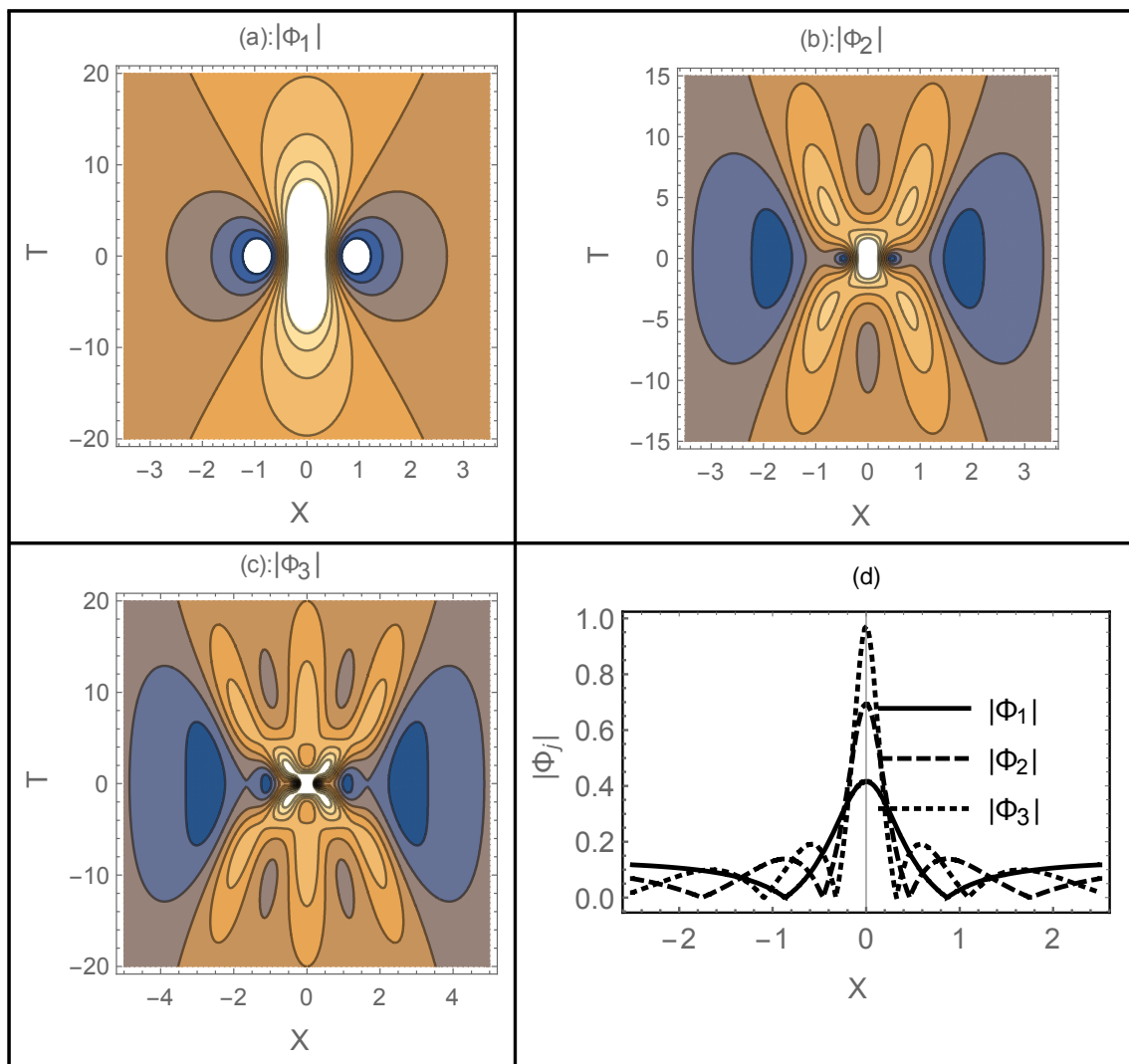

Figure 8. A comparison between different orders of RW solution. (**a**) The first-order RWs $|\Phi_1|$, (**b**) the second-order RWs $|\Phi_2|$, (**c**) the third-order RWs $|\Phi_3|$, and (**d**) the first three-orders of RWs $|\Phi_{1,2,3}|$. Here, $(\mu, \sigma, q, r, k) = (0.3, 0.2, 6, 1.2, 0.99)$.
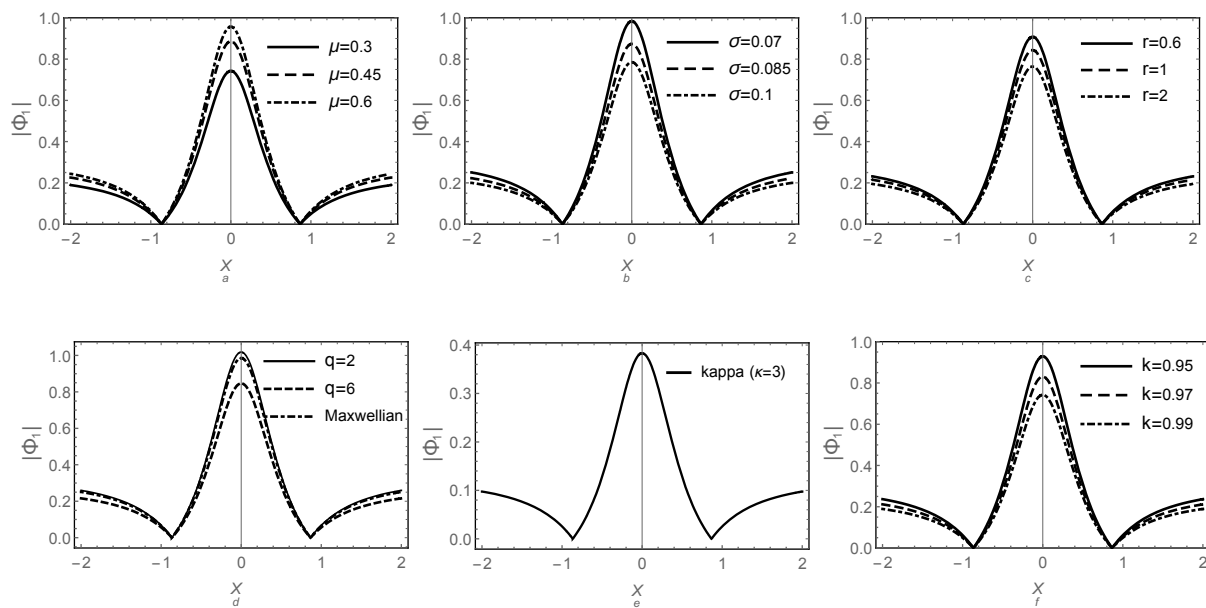
Figure 9. The profile of first-order RWs $|\Phi_1|$ is plotted for (**a**) $(\sigma, q, r, k) = (0.1, 3, 1.6, 0.99)$ with varying μ, (**b**) $(\mu, q, r, k) = (0.3, 3, 1.6, 0.98)$ with varying σ, (**c**) $(\mu, \sigma, q, k) = (0.3, 0.1, 3, 0.98)$ with varying r, (**d**) $(\mu, \sigma, r, k) = (0.3, 0.1, 0.6, 0.98)$ with varying q for solid and dashed curves, $(\mu, \sigma, k) = (0.3, 0.1, 0.98)$ for dotted-dashed curve (Maxwellian distribution $r = 0$, $q \to \infty$) (**e**) $(\mu, \sigma, k) = (1.2, 0.1, 0.98)$ for kappa distribution, $r = 0$, $q \to \kappa + 1$, $\kappa = 3$ and (**f**) $(\mu, \sigma, q, r) = (0.3, 0.1, 3, 1.6)$ with varying k.

7. Conclusions

The propagation of electrostatic electron-acoustic (un)modulated waves in a non-Maxwellian plasma consisting of two-temperature electrons (hot electrons following (r, q) distribution and cold inertial electrons) and stationary positive ions were investigated. The Sagdeev potential approach was used to reduce the governing fluid equations to the energy equation for studying the unmodulated arbitrary amplitude solitary waves. It was shown that changing the plasma parameters and the indices (r, q) of the hot electron distribution function alters the existence domains of the formation of electron-acoustic solitary structures. The limiting cases of kappa and Maxwellian distributions show that solitons in kappa distribution are permitted only for smaller values of Mach numbers. The profile of unmodulated arbitrary amplitude solitary waves is strongly dependent on the plasma parameters and the electron distribution function. It has been found that the Sagdeev potential corresponding to kappa distribution is deepest and widest, intermediate for Maxwellian, whereas it is least from flat-topped distribution with Maxwellian tail. It was also shown that enhancing the number of electrons in both the low and high regions of phase space density by increasing the spectral indices r and q enervate the amplitude of the EASWs by comparison with their Maxwellian counterparts. Furthermore, the derivative expansion method were employed to obtain the nonlinear Schrödinger equation (NLSE) for investigating the modulated structures, including rogue waves, super rogue waves, and breathers. Employing the criteria of modulational instability, the existence domain of RWs and breathers were determined precisely. The effect of the relevant physical parameters on the profile of the RWs was reported, where the Maxwellian and kappa distributions were also investigated. It was shown that the amplitude of the rogue waves is highest for Maxwellian distributed electrons and intermediate for generalized (r, q) distributed electrons, whereas it is minimum for kappa distributed electrons. Moreover, it was observed that the impact of all physical plasma parameters on the super (second- and third-order) RWs have the same qualitative behavior, but the super RWs become more spiky (large amplitude and narrower width) than the first-order RWs. The results obtained here may help us to understand the mechanism of the propagation of nonlinear electrostatic (un)modulated structures in laboratory and space plasmas.

References

1. Fried, B.D.; Gould, R.W. Longitudinal ion oscillations in a hot plasma. *Phys. Fluids* **1961**, *4*, 139–147. [CrossRef]
2. Henry, D.; Treumann, R.A. Propagation of electronic longitudinal modes in a non-Maxwellian plasma. *J. Plasma Phys.* **1972**, *8*, 311–319. [CrossRef]
3. Matsumoto, H.; Kojima, H.; Miyatake, T.; Omura, Y.; Okada, M.; Nagano, I.; Tsutsui, M. Electrostatic solitary waves (ESW) in the magnetotail: BEN wave forms observed by GEOTAIL. *Geophys. Res. Lett.* **1994**, *21*, 2915–2918. [CrossRef]
4. Bale, S.D.; Kellogg, P.J.; Larsen, D.E.; Lin, R.P.; Goetz, K.; Lepping, R.P. Bipolar electrostatic structures in the shock transition region: Evidence of electron phase space holes. *Geophys. Res. Lett.* **1998**, *25*, 2929–2932. [CrossRef]
5. Pickett, J.S.; Chen, L.J.; Kahler, S.W.; Santolik, O.; Goldstein, M.L.; Lavraud, B.; Décréau, P.M.E.; Kessel, R.; Lucek, E.; Lakhina, G.S.; et al. On the generation of solitary waves observed by Cluster in the near-Earth magnetosheath. *Nonlinear Process. Geophys.* **2005**, *12*, 181–193. [CrossRef]
6. Tokar, R.L.; Gary, S.P. Electrostatic hiss and the beam driven electron acoustic instability in the dayside polar cusp. *Geophys. Res. Lett.* **1984**, *11*, 1180–1183. [CrossRef]
7. Pottelette, R.; Ergun, R.E.; Treumann, R.A.; Berthomier, M.; Carlson, C.W.; McFadden, J.P.; Roth, I. Modulated electron-acoustic waves in auroral density cavities: FAST observations. *Geophys. Res. Lett.* **1999**, *26*, 2629–2632. [CrossRef]
8. Pickett, J.S.; Kahler, S.W.; Chen, L.J.; Huff, R.L.; Santolik, O.; Khotyaintsev, Y.; Décréau, P.M.E.; Winningham, D.; Frahm, R.; Goldstein, M.L.; et al. Solitary waves observed in the auroral zone: The Cluster multi-spacecraft perspective. *Nonlinear Process. Geophys.* **2004**, *11*, 183–196. [CrossRef]
9. Dubouloz, N.; Pottelette, R.; Malingre, M.; Treumann, R.A. Generation of broadband electrostatic noise by electron acoustic solitons. *Geophys. Res. Lett.* **1991**, *18*, 155–158. [CrossRef]
10. Lakhina, G.S.; Singh, S.V.; Kakad, A.P.; Pickett, J.S. Generation of electrostatic solitary waves in the plasma sheet boundary layer. *J. Geophys. Res. Space Phys.* **2011**, *116*. [CrossRef]
11. Dillard, C.S.; Vasko, I.Y.; Mozer, F.S.; Agapitov, O.V.; Bonnell, J.W. Electron-acoustic solitary waves in the Earth's inner magnetosphere. *Phys. Plasmas* **2018**, *25*, 022905. [CrossRef]
12. Watanabe, K.; Taniuti, T. Electron-Acoustic Mode in a Plasma of Two-Temperature Electrons. *J. Phys. Soc. Jpn.* **1977**, *43*, 1819–1820. [CrossRef]
13. Stix, T.H. *Waves in Plasmas*; AIP: New York, NY, USA, 1992.
14. Gary, S.P.; Tokar, R.L. The electron-acoustic mode. *Phys. Fluids* **1985**, *28*, 2439–2441. [CrossRef]
15. Berthomier, M.; Pottelette, R.; Malingre, M.; Khotyaintsev, Y. Electron-acoustic solitons in an electron-beam plasma system. *Phys. Plasmas* **2000**, *7*, 2987–2994. [CrossRef]
16. Mace, R.L.; Hellberg, M.A. The Korteweg–de Vries–Zakharov–Kuznetsov equation for electron-acoustic waves. *Phys. Plasmas* **2001**, *8*, 2649–2656. [CrossRef]
17. Mamun, A.A.; Shukla, P.K.; Stenflo, L. Obliquely propagating electron-acoustic solitary waves. *Phys. Plasmas* **2002**, *9*, 1474–1477. [CrossRef]
18. Shukla, P.K.; Mamun, A.A.; Eliasson, B. 3D electron-acoustic solitary waves introduced by phase space electron vortices in magnetized space plasmas. *Geophys. Res. Lett.* **2004**, *31*, L07803. [CrossRef]
19. Singh, K.; Saini, N.S. Effect of anisotropic pressure on electron acoustic oscillatory and monotonic shocks in superthermal magnetoplasma. *Radio Sci.* **2019**, *54*, 1192–1203. [CrossRef]
20. Mace, R.L.; Hellberg, M.A. A dispersion function for plasmas containing superthermal particles. *Phys. Plasmas* **1995**, *2*, 2098–2109. [CrossRef]
21. Summers, D.; Thorne, R.M.; Matsumoto, H. Evaluation of the modified plasma dispersion function for half-integral indices. *Phys. Plasmas* **1996**, *3*, 2496–2501. [CrossRef]
22. Abid, A.A.; Khan, M.Z.; Lu, Q.; Yap, S.L. A generalized AZ-non-Maxwellian velocity distribution function for space plasmas. *Phys. Plasmas* **2017**, *24*, 033702. [CrossRef]

23. Vasyliunas, V.M. A survey of low-energy electrons in the evening sector of the magnetosphere with OGO 1 and OGO 3. *J. Geophys. Res.* **1968**, *73*, 2839–2884. [CrossRef]

24. Feldman, W.C.; Anderson, R.C.; Bame, S.J.; Gary, S.P.; Gosling, J.T.; McComas, D.J.; Thomsen, M.F.; Paschmann, G.; Hoppe, M.M. Electron velocity distributions near the Earth's bow shock. *J. Geophys. Res. Space Phys.* **1983**, *88*, 96–110.

25. Masood, W.; Schwartz, S.J.; Maksimovic, M.; Fazakerley, A.N. Electron velocity distribution and lion roars in the magnetosheath. *Ann. Geophys.* **2006**, *24*, 1725–1735. [CrossRef]

26. Masood, W.; Schwartz, S.J. Observations of the development of electron temperature anisotropies in Earth's magnetosheath. *J. Geophys. Res.* **2008**, *106*, A01216. [CrossRef]

27. Asano, Y.; Nakamura, R.; Shinohara, I.; Fujimoto, M.; Takada, T.; Baumjohann, W.; Owen, C.J.; Fazakerley, A.N.; Runov, A.; Nagai, T.; et al. Electron flat-top distributions around the magnetic reconnection region. *J. Geophys. Res. Space Phys.* **2008**, *113*. [CrossRef]

28. Qureshi, M.N.; Shah, H.A.; Murtaza, G.; Schwartz, S.J.; Mahmood, F. Parallel propagating electromagnetic modes with the generalized distribution function. *Phys. Plasmas* **2004**, *11*, 3819–3829. [CrossRef]

29. Qureshi, M.N.; Nasir, W.; Masood, W.; Yoon, P.H.; Shah, H.A.; Schwartz, S.J. Terrestrial lion roars and non-Maxwellian distribution. *J. Geophys. Res. Space Phys.* **2014**, *119*, 10059–10067. [CrossRef]

30. Shah, K.H.; Qureshi, M.N.; Masood, W.; Shah, H.A. Electron acoustic nonlinear structures in planetary magnetospheres. *Phys. Plasmas* **2018**, *25*, 042303. [CrossRef]

31. Sagdeev, R.Z. *Reviews of Plasma Physics*; Leontovich, M.A., Ed.; Consultants Bureau: New York, NY, USA, 1966.

32. Albalawi, W.; El-Tantawy, S.A.; Salas, A.H. On the rogue wave solution in the framework of a Korteweg–de Vries equation. *Results Phys.* **2021**, *30*, 104847. [CrossRef]

33. Tiofack, C.G.L.; Douanla, D.V.; Mohamadou, A.; Ismaeel, S.M.E.; El-Tantawy, S.A. Dust-acoustic modulated structures in self-gravitating magnetized electron depleted dusty plasmas: Multi-rogue waves and dark soliton collisions. *Eur. Phys. J. Plus* **2021**, *136*, 699. [CrossRef]

34. Aljahdaly, N.H.; El-Tantawy, S.A. Simulation study on nonlinear structures in nonlinear dispersive media. *Chaos Interdiscip. J. Nonlinear Sci.* **2020**, *30*, 053117. [CrossRef]

35. Irfan, M.; Ali, S.; El-Tantawy, S.A.; Ismaeel, S.M.E. Three dimensional ion-acoustic rogons in quantized anisotropic magnetoplasmas with trapped/untrapped electrons. *ChaosInterdiscip. J. Nonlinear Sci.* **2019**, *29*, 103133. [CrossRef] [PubMed]

36. El-Tantawy, S.A.; Salas, A.H.; Alharthi, M.R. On the Analytical and Numerical Solutions of the Linear Damped NLSE for Modeling Dissipative Freak Waves and Breathers in Nonlinear and Dispersive Mediums: An Application to a Pair-Ion Plasma. *Front. Phys.* **2021**, *9*, 580224. [CrossRef]

37. Salas, A.H.; El-Tantawy, S.A.; Castillo, H.J.E. The hybrid finite difference and moving boundary methods for solving a linear damped nonlinear Schrödinger equation to model rogue waves and breathers in plasma physics. *Math. Probl. Eng.* **2020**, *2020*, 6874870. [CrossRef]

38. Bansal, S.; Gill, T.S.; Aggarwal, M. Oblique modulation of electron acoustic waves in superthermal plasma. *Phys. Scr.* **2019**, *94*, 105603. [CrossRef]

39. Peregrine, D.H. Water waves, nonlinear Schrödinger equations and their solutions. *ANZIAM J.* **1983**, *25*, 16–43. [CrossRef]

40. Akhmediev, N.; Ankiewicz, A.; Taki, M. Waves that appear from nowhere and disappear without a trace. *Phys. Lett. A* **2009**, *373*, 675–678. [CrossRef]

41. Akhmediev, N.; Ankiewicz, A.; Soto-Crespo, J.M. Rogue waves and rational solutions of the nonlinear Schrödinger equation. *Phys. Rev. E* **2009**, *80*, 026601. [CrossRef] [PubMed]

42. Ankiewicz, A.; Devine, N.; Akhmediev, N. Are rogue waves robust against perturbations? *Phys. Lett. A* **2009**, *373*, 3997–4000. [CrossRef]

43. Kuznetsov, E.A. Solitons in a parametrically unstable plasma. *Akad. Nauk. SSSR Dokl.* **1977**, *236*, 575–577.

44. Ma, Y.C. The perturbed plane-wave solutions of the cubic Schrödinger equation. *Stud. Appl. Math.* **1979**, *60*, 43–58. [CrossRef]

45. Ruderman, M.S. Freak waves in laboratory and space plasmas. *Eur. Phys. J. Spec. Top.* **2010**, 185, 57–66. [CrossRef]

46. El-Bedwehy, N.A. Freak waves in GaAs semiconductor. *Physica B* **2014**, *442*, 114–117. [CrossRef]

47. El-Tantawy, S.A.; Alshehri, M.H.; Duraihem, F.Z.; El-Sherif, L.S. Dark soliton collisions and method of lines approach for modeling freak waves in a positron beam plasma having superthermal electrons. *Results Phys.* **2020**, *19*, 103452. [CrossRef]

48. Singh, K.; Saini, N.S. The evolution of rogue wave triplets and super rogue waves in superthermal polarized space dusty plasma. *Phys. Plasmas* **2019**, *26*, 113702. [CrossRef]

49. Almutlak, S.A.; El-Tantawy, S.A.; Shan, S.A.; Ismaeel, S.M. Multidimensional freak waves in electron depleted dusty magneto-plasmas having superthermal ion with two temperatures. *Eur. Phys. J. Plus* **2019**, *134*, 513. [CrossRef]

50. Akhtar, N.; El-Tantawy, S.A.; Mahmood, S.; Wazwaz, A.-M. On the dynamics of dust-acoustic and dust-cyclotron freak waves in a magnetized dusty plasma. *Rom. Rep. Phys.* **2019**, *71*, 403.

51. El-Tantawy, S.A.; Wazwaz, A.M. Anatomy of modified Korteweg–de Vries equation for studying the modulated envelope structures in non-Maxwellian dusty plasmas: Freak waves and dark soliton collisions. *Phys. Plasmas* **2018**, *25*, 092105. [CrossRef]

52. El-Tantawy, S.A.; Shan, S.A.; Akhtar, N.; Elgendy, A.T. Impact of electron trapping in degenerate quantum plasma on the ion-acoustic breathers and super freak waves. *Chaos Solitons Fract.* **2018**, *113*, 356–364. [CrossRef]

53. El-Tantawy, S.A.; Ali, S.; Maroof, R.; Wazwaz, A.-M.; El-Labany, S.K. On the super freak waves in multicomponent plasmas having two-negative ions: $Xe^+ - F^- - SF_6^-$ and $Ar^+ - F^- - SF_6^-$ plasmas. *Indian J. Phys.* **2017**, *91*, 939–946. [CrossRef]

54. El-Tantawy, S.A.; Aboelenen, T. Simulation study of planar and nonplanar super rogue waves in an electronegative plasma: Local discontinuous Galerkin method. *Phys. Plasmas* **2017**, *24*, 052118. [CrossRef]

55. El-Tantawy, S.A. Ion-acoustic waves in ultracold neutral plasmas: Modulational instability and dissipative rogue waves. *Phys. Lett. A* **2017**, *381*, 787–791. [CrossRef]

56. El-Tantawy, S.A.; Wazwaz, A.M.; Ali Shan, S. On the nonlinear dynamics of breathers waves in electronegative plasmas with Maxwellian negative ions. *Phys. Plasmas* **2017**, *24*, 022105. [CrossRef]

57. Turing, A. Philosophical the royal biological transqfctions society sciences. *Philos. Trans. R. Soc. Lond. B* **1952**, *237*, 37–72.

58. Benjamin, T.B.; Feir, J.E. The disintegration of wave trains on deep water Part 1. Theory. *J. Fluid Mech.* **1967**, *27*, 417–430. [CrossRef]

59. Solli, D.R.; Ropers, C.; Koonath, P.; Jalali, B. Optical rogue waves. *Nature* **2007**, *450*, 1054–1057. [CrossRef] [PubMed]

60. Bludov, Y.V.; Konotop, V.V.; Akhmediev, N. Matter rogue waves. *Phys. Rev. A* **2009**, *80*, 033610. [CrossRef]

61. Chowdhury, N.A.; Mannan, A.; Mamun, A.A. Rogue waves in space dusty plasmas. *Phys. Plasmas* **2017**, *24*, 113701. [CrossRef]

62. Dysthe, K.; Krogstad, H.E.; Müller, P. Oceanic rogue waves. *Annu. Rev. Fluid Mech.* **2008**, *40*, 287–310. [CrossRef]

63. Stenflo, L.; Marklund, M. Rogue waves in the atmosphere. *J. Plasma Phys.* **2010**, *76*, 293–295. [CrossRef]

64. Bailung, H.; Sharma, S.K.; Nakamura, Y. Observation of Peregrine solitons in a multicomponent plasma with negative ions. *Phys. Rev. Lett.* **2011**, *107*, 255005. [CrossRef]

65. Merriche, A.; Tribeche, M. Electron-acoustic rogue waves in a plasma with Tribeche–Tsallis–Cairns distributed electrons. *Ann. Phys.* **2017**, *376*, 436–447. [CrossRef]

66. Ullah, S.; Masood, W.; Siddiq, M.; Rizvi, H. Oblique modulation and envelope excitations of nonlinear ion sound waves with cubic nonlinearity and generalized (r, q) distribution. *Phys. Scr.* **2019**, *94*, 125604. [CrossRef]

67. Ullah, S.; Masood, W.; Siddiq, M. Electron acoustic envelope solitons in non-Maxwellian plasmas. *Eur. Phys. J. D* **2020**, *74*, 1–9. [CrossRef]

68. Liu, J.G.; Xiong, W.P. Multi-wave, breather wave and lump solutions of the Boiti–Leon–Manna–Pempinelli equation with variable coefficients. *Results Phys.* **2020**, *19*, 103532. [CrossRef]

69. Singh, K.; Saini, N.S. Breather Structures and Peregrine Solitons in a Polarized Space Dusty Plasma. *Front. Phys.* **2020**, *8*, 602229. [CrossRef]

70. Kibler, B.; Fatome, J.; Finot, C.; Millot, G.; Genty, G.; Wetzel, B.; Akhmediev, N.; Dias, F.; Dudley, J.M. Observation of Kuznetsov–Ma soliton dynamics in optical fiber. *Sci. Rep.* **2012**, *2*, 1–5. [CrossRef]

71. Danehkar, A.; Saini, N.S.; Hellberg, M.A.; Kourakis, I. Electron-acoustic solitary waves in the presence of a suprathermal electron component. *Phys. Plasmas* **2011**, *18*, 072902. [CrossRef]

72. Lakhina, G.S.; Singh, S.V.; Rubia, R.; Sreeraj, T. A review of nonlinear fluid models for ion-and electron-acoustic solitons and double layers: Application to weak double layers and electrostatic solitary waves in the solar wind and the lunar wake. *Phys. Plasmas* **2018**, *25*, 080501. [CrossRef]

73. Verheest, F.; Hellberg, M.A. Effects of hot electron inertia on electron-acoustic solitons and double layers. *Phys. Plasmas* **2015**, *22*, 072303. [CrossRef]

74. Kourakis, I.; Shukla, P.K. Modulational instability and localized excitations of dust-ion acoustic waves. *Phys. Plasmas* **2003**, *10*, 3459. [CrossRef]

75. Xue, J.K. Modulation of dust acoustic waves with non-adiabatic dust charge fluctuations. *Phys. Lett. A* **2003**, *320*, 226–233. [CrossRef]